

## Electronic Supplementary Information

### **Metallic oxide nanocrystals with near-infrared plasmon resonance for efficient, stable and biocompatible photothermal cancer therapy**

Kang Dou, ‡<sup>a</sup> Wenwen Zhu, ‡<sup>b</sup> Yousheng Zou, \*<sup>a</sup> Yu Gu, <sup>a</sup> Jubin Li, <sup>a</sup> Shengli Zhang, <sup>a</sup> Zhuang Liu, \*<sup>b</sup> and Haibo Zeng \*<sup>a</sup>

<sup>a</sup> *MIIT Key Laboratory of Advanced Display Materials and Devices, Institute of Optoelectronics & Nanomaterials, School of Materials Science and Engineering, Nanjing University of Science and Technology, Nanjing 210094, China.*

<sup>b</sup> *Institute of Functional Nano & Soft Materials Laboratory (FUNSOM), Soochow University, Suzhou 215123, China.*

\*Correspondence and requests for material to Yousheng Zou or Haibo Zeng or Zhuang Liu, Email address: yshzou75@njust.edu.cn; zliu@suda.edu.cn; zeng.haibo@njust.edu.cn

‡ These authors contribute to this work equally.

† Electronic supplementary information (ESI) available: Synthesis mechanism scheme of MoO<sub>2</sub> nanocrystals, Simulation of MoO<sub>2</sub> nanocrystals absorption spectrum.

**KEYWORDS:** nanocrystal, MoO<sub>2</sub>, localized surface plasmon resonance, photothermal therapy

## The synthesis mechanism scheme of MoO<sub>2</sub> nanocrystals

When pulsed laser is induced to molybdenum target in the mixed solution of ethanol and hydrogen peroxide, a plasma plume containing many different Mo ions and other active ion species such as H<sup>+</sup>, OH<sup>-</sup> and O<sup>2-</sup> resulted from the mixed solution are formed in less than 100ns under high temperature, high density, and high pressure.<sup>1</sup> These active ion species can combine with Mo ions to form different molybdenum oxides,<sup>2</sup> such as MoO<sub>2</sub><sup>+</sup>, MoO<sub>3</sub><sup>+</sup>, MoO<sup>+</sup>, Mo<sub>2</sub>O<sub>5</sub><sup>+</sup>, Mo<sub>3</sub>O<sub>8</sub><sup>+</sup>, etc. The subsequent ultrasonic and adiabatic expansion of the plasma leads to cooling of the molybdenum oxide plume region and hence the formation of molybdenum oxide clusters.<sup>3</sup> The concentration and species of molybdenum oxides clusters depend on the volume ratio of ethanol and H<sub>2</sub>O<sub>2</sub>. The formed cluster further interacts with solvent to induce nanoparticles through chemical reactions. The structure, morphology and chemical composition of the colloid containing the above nanoparticles vary with different ablation media, as well as the interaction duration between laser and nanoparticles. Thus the morphology, phase composition and microstructure of molybdenum oxides can be regulated by the chemical composition of ablation solution and ablation time.

The synthesized colloid containing various molybdenum oxides nanoparticles was served as the precursor for the subsequent solvothermal process. The size, concentration and species of the corresponding molybdenum oxides nanoparticles in the colloid varied when the volume ratio of ethanol and H<sub>2</sub>O<sub>2</sub> changed from 2:1 to 1:1. Under the same process conditions of solvothermal, the varied precursor mainly affected the nucleation and the preferred orientation growth of molybdenum oxide nanostructures during the solvothermal process, resulting in the morphology dependence of the prepared samples on the volume ratio of ethanol and H<sub>2</sub>O<sub>2</sub> in LAL media. Therefore, the precursor variation resulted from the decrease of volume ratio of ethanol and H<sub>2</sub>O<sub>2</sub> resulted in transforming MoO<sub>2</sub> NCs from irregular nanosphere to nanorod.

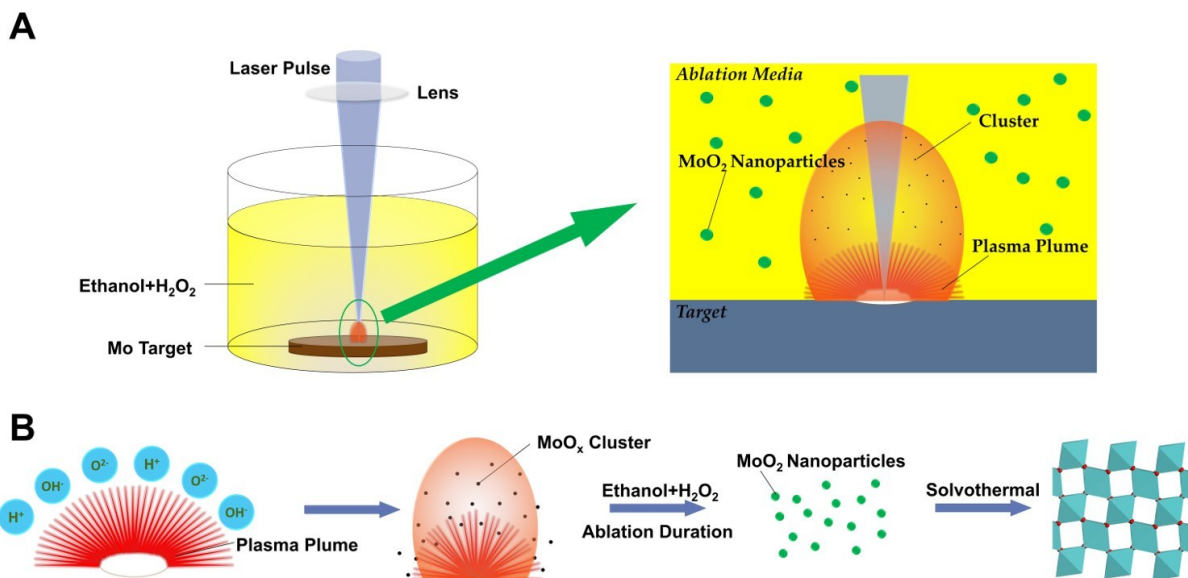


**Figure S1** Synthesis mechanism scheme of  $\text{MoO}_2$  nanocrystals. A) Sketch of laser ablation in liquid process. B) Growth process illustration of crystalline monoclinic  $\text{MoO}_2$  nanocrystals.

## XPS and Raman spectra of $\text{MoO}_2$ nanocrystals

Both  $\text{MoO}_2$  irregular nanospheres and nanorods were characterized by XPS and Raman spectra, which are shown in Figure S2. Raman spectra of both  $\text{MoO}_2$  irregular nanospheres and nanorods exhibit features at 199, 225, 353, 489, 562 and 731  $\text{cm}^{-1}$ , which have previously been reported to be characteristic of monoclinic  $\text{MoO}_2$ .<sup>4</sup> Besides, another two weaker peaks located at 820 and 989  $\text{cm}^{-1}$  are also observed in the spectra, which are assigned to the doubly coordinated oxygen ( $\text{Mo}_2\text{-O}$ ) stretching and the terminal oxygen ( $\text{Mo=O}$ ) stretching mode respectively.

According to the XPS spectra analysis (Figure S2C and D),  $\text{MoO}_2$  NCs with both shapes exhibit two sharp peaks located at 229.47 eV and 232.62 eV, which are corresponding to the  $3d_{5/2}$  and  $3d_{3/2}$  orbit of  $\text{Mo}^{4+}$ , respectively. Two weak peaks located at 230.91 eV and 234 eV are attributed to  $\text{Mo}^{5+}$ . Therefore, the as-synthesized  $\text{MoO}_2$  NCs are mainly composed of  $\text{Mo}^{4+}$  with minor  $\text{Mo}^{5+}$  that maybe caused by the existence of O interstitial atom. However, no

Mo<sup>6+</sup> peaks appear in the spectra, indicating that Mo exhibits reduction state in the MoO<sub>2</sub> nanocrystals fabricated by the combination of laser ablation in liquid and solvothermal method.

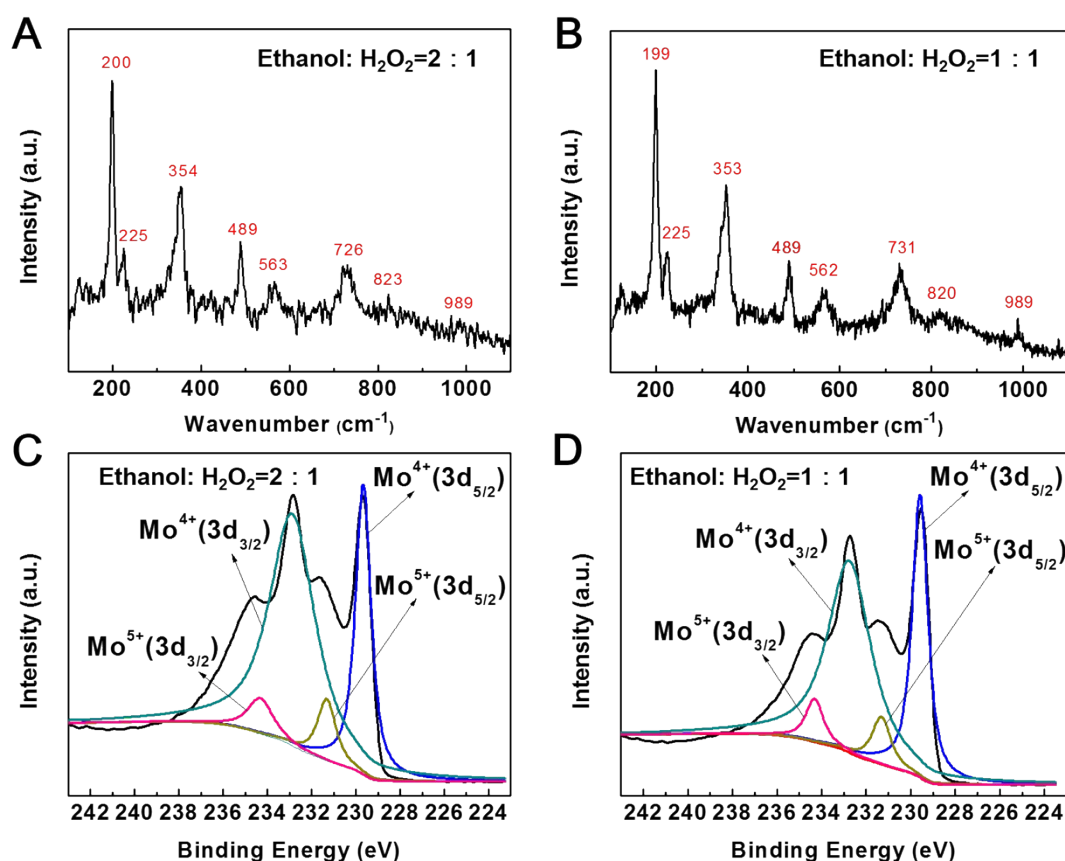


**Figure S2** A) Raman spectrum of MoO<sub>2</sub> irregular nanoparticles synthesized with Ethanol: H<sub>2</sub>O<sub>2</sub> volume ratio of 2:1. B) Raman spectrum of MoO<sub>2</sub> nanorods synthesized with Ethanol: H<sub>2</sub>O<sub>2</sub> volume ratio of 1:1. C) XPS spectrum of MoO<sub>2</sub> irregular nanoparticles synthesized with Ethanol: H<sub>2</sub>O<sub>2</sub> volume ratio of 2:1. D) XPS spectrum of MoO<sub>2</sub> nanorods synthesized with Ethanol: H<sub>2</sub>O<sub>2</sub> volume ratio of 1:1.

## Simulation of MoO<sub>2</sub> nanocrystals absorption spectrum

The optical constants of MoO<sub>2</sub> are described by Drude model:

$$\begin{aligned}\varepsilon(\omega) &= \varepsilon_\infty - \frac{\omega_p^2}{\omega^2 + i\gamma\omega} = \varepsilon' + i\varepsilon'' \\ \varepsilon' &= \varepsilon_\infty - \frac{\omega_p^2}{\omega^2 + \gamma^2} \quad \varepsilon'' = \frac{\omega_p^2}{\omega^2 + \gamma^2} \frac{\gamma}{\omega}\end{aligned}\tag{S1}$$

In which,  $\omega_p = [nq^2/m_e\varepsilon_0]^{1/2}$  is the plasma frequency,  $n$  is the carrier concentration,  $q$  is the elementary charge,  $m_e$  is the effective mass,  $\varepsilon_0$  is the vacuum permittivity.  $\gamma$  is the collision frequency. The absorption cross section (the scattering cross section is ignored here) which mimics the line shape of the experimental absorption spectrum is written as:<sup>5</sup>

$$\sigma(\omega) = 9 \frac{2\pi}{\lambda} \varepsilon_m^{3/2} \frac{\varepsilon''}{(\varepsilon' + 2\varepsilon_m)^2 + \varepsilon''^2} V\tag{S2}$$

In which  $\varepsilon_m$  is the permittivity of the solvent.  $\lambda$  is the wavelength of light and  $V$  is the particle volume. By adjusting  $\omega_p$  and  $\gamma$ , one can match the calculated spectrum  $\sigma(\omega)$  with the experimental one for only one simulation. Then the same material parameter  $\omega_p$  is used for other simulations with different surrounding mediums and only some minor adjustment of  $\gamma$  is allowed for achieving better fitting. For rod-like nanocrystals, an additional shape factor is added into the simulation as follows:

$$\sigma(\omega) = 9 \frac{2\pi}{\lambda} \varepsilon_m^{3/2} \frac{\varepsilon''}{[f\varepsilon' + (3-f)\varepsilon_m]^2 + (f\varepsilon'')^2} V\tag{S3}$$

$f$  is the shape factor and is defined as:

$$f_i = \frac{3}{2} a_1 a_2 a_3 \int_0^\infty \frac{dq}{(a_i^2 + q) \sqrt{(a_1^2 + q)(a_2^2 + q)(a_3^2 + q)}}\tag{S4}$$

For a rod with length  $l$ , diameter  $d$ , the three axes  $a_1, a_2, a_3$  are defined as  $a_1=d, a_2=d, a_3=l$  respectively. The shape factor  $f_1$  was used for the transverse resonance mode. It is worth noting that the material parameters used for the simulations of rod-like nanocrystals is the same as that extracted for spherical particles. No fitting of any parameters were involved and the simulation spectrums were calculated and compared with the experimental ones directly.

## Calculation of the molar extinction coefficient

To evaluate the NIR photo-absorption capability of MoO<sub>2</sub> irregular nanospheres, the extinction coefficient  $\alpha(\lambda)$  of the MoO<sub>2</sub> irregular nanospheres is given, according to the Lambert-Beer Law:

$$A(\lambda) = \alpha LC \quad (\text{S5})$$

where  $A$  is the absorbance at a wavelength  $\lambda$ ,  $\alpha$  is the extinction coefficient,  $L$  is path-length (1 cm), and  $C$  is the concentration of the MoO<sub>2</sub> irregular nanospheres (g/L). The extinction coefficient  $\alpha$  is determined according to the linear dependence of normalized absorbance over the cell length on the concentration.

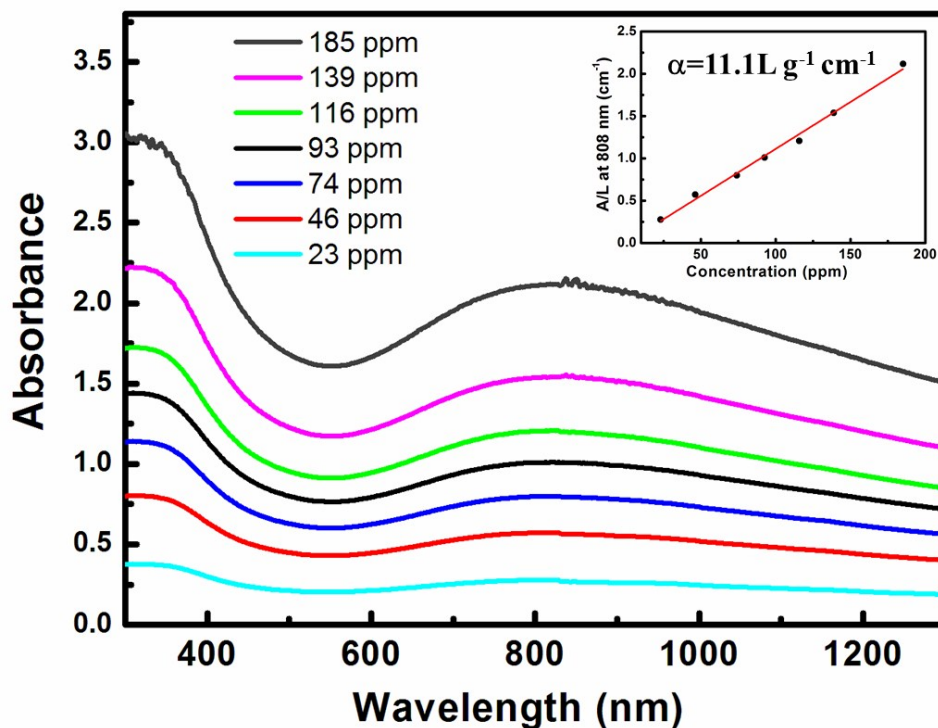


**Figure S3** Absorbance spectra of MoO<sub>2</sub> NCs dispersed in water at varied concentrations. Inset: Linear fitting chart of normalized absorbance at  $\lambda=808$  nm *versus* concentrations of MoO<sub>2</sub> solutions.

The normalized adsorption intensity over the length of the cell ( $A/L$ ) at  $\lambda=808$  nm at various concentrations ( $C$ ) was determined. The linear dependence of  $A/L$  on the concentration can be obtained according to the Lambert-Beer law, as shown in Figure S3. The extinction coefficient at 808 nm was calculated to be  $11.1 \text{ L g}^{-1} \text{ cm}^{-1}$  (Figure S3 inset), and the corresponding molar extinction coefficient ( $\varepsilon$ ) was  $1420 \text{ M}^{-1} \text{ cm}^{-1}$ .

## Calculation of the photothermal conversion efficiency

The photothermal conversion efficiency ( $\eta$ ) of the  $\text{MoO}_2$  irregular nanospheres was measured by a modified method similar to the previous report.<sup>6,7</sup> The temperature change of the  $\text{MoO}_2$  aqueous solution (25 ppm) was recorded as a function of time under continuous irradiation of 808nm NIR laser at a power of  $0.8 \text{ W/cm}^2$ , in which the irradiation lasted for 240 s, and then the laser was shut off (Figure S4A).

Following Roper's report,<sup>6</sup> the photothermal conversion efficiency was calculated using the following equation (S6).

$$\eta = \frac{hS(T_{Max} - T_{Surr}) - Q_{Dis}}{I(1 - 10^{-A_{808}})} \quad (\text{S6})$$

where  $h$  is the heat transfer coefficient,  $S$  is the surface area of the sample cuvette, and the value of  $hS$  is obtained from the linear time data from the cooling stage *versus* negative natural logarithm of driving force temperature (Figure S4B). Thus, the  $hS$  was calculated to be  $11.3 \text{ mW/}^\circ\text{C}$ .  $T_{Max}$  and  $T_{Surr}$  are the equilibrium temperature and ambient surrounding temperature, respectively. And  $(T_{Max}-T_{Surr})$  was calculated to be  $42.1^\circ\text{C}$  according to Figure S4A. In addition,  $Q_{Dis}$  expresses the heat dissipated due to light absorption by the pure water without  $\text{MoO}_2$  irregular nanospheres, which was measured independently and found to be  $0.1512 \text{ mW}$ .  $I$  is the incident laser power ( $2512 \text{ mW}$ ),  $A_{808}$  is the absorbance ( $0.4704$ ) of  $\text{MoO}_2$  irregular nanospheres at 808 nm. Substituting these values into equation (S6), the 808

nm laser photothermal conversion efficiency ( $\eta$ ) of MoO<sub>2</sub> irregular nanospheres can be calculated to be 28.6%.

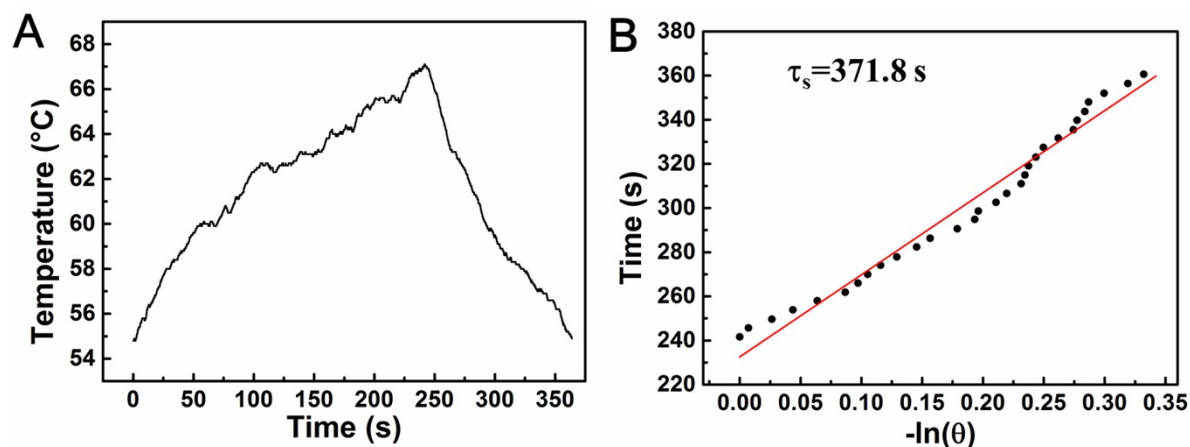


**Figure S4** A) Photothermal effect of aqueous dispersion of MoO<sub>2</sub> irregular nanospheres (25 ppm) under irradiation with the NIR laser (808 nm, 0.8 W/cm<sup>2</sup>) for one on/off cycle. B) Time constant for heat transfer from the system is determined to be  $\tau_s = 371.8$  s by applying the linear time data from the cooling period (after 240 s) versus negative natural logarithm of driving force temperature, which is obtained from the cooling stage of Figure S4(A).

## Notes and references

- 1 D. Kim and H. Lee, *J. Appl. Phys.*, 2001, **89**, 5703–5706.
- 2 P. Liu, Y. Liang, X. Z. Lin, C. X. Wang and G. W. Yang, *ACS Nano*, 2011, **5**, 4748–4755.
- 3 H. B. Zeng, Z. Li, W. P. Cai, B. Cao, P. S. Liu and S. K. Yang, *J. Phys. Chem. B.*, 2007, **111**, 14311–14317.
- 4 M. A. Camacho-López, L. Escobar-Alarcón, M. Picquart, R. Arroyo, G. Córdoba and E. Haro-Poniatowski, *Opt. Mater.*, 2011, **33**, 480–484.
- 5 S. A. Maier, *Plasmonics: Fundamentals and Applications*. Springer Berlin, 2007, pp. 49–74.
- 6 D. K. Roper, W. Ahn and M. Hoepfner, *J. Phys. Chem. C*, 2007, **111**, 3636–3641.



7 H. Lin, X. G. Wang, L. D. Yu, Y. Chen and J. L. Shi, *Nano Lett.*, 2017, **17**, 384–391.